Article

pubs.acs.org/Biomac

Enhanced Redifferentiation of Chondrocytes on Microperiodic Silk/Gelatin Scaffolds: Toward Tailor-Made Tissue Engineering

Sanskrita Das,[†,‡] Falguni Pati,[†] Shibu Chameettachal,[†] Shikha Pahwa,[†] Alok R. Ray,[‡] Santanu Dhara,[§] and Sourabh Ghosh*[,†]

[†]Department of Textile Technology, Indian Institute of Technology, New Delhi, India

[‡]Centre for Biomedical Engineering, Indian Institute of Technology and All India Institute of Medical Sciences, New Delhi, India

[§]School of Medical Science and Technology, Indian Institute of Technology, Kharagpur, India

Supporting Information

ABSTRACT: Direct-write assembly allows rapid fabrication of complex three-dimensional (3D) architectures, such as scaffolds simulating anatomical shapes, avoiding the need for expensive lithographic masks. However, proper selection of polymeric ink composition and tailor-made viscoelastic properties are critically important for smooth deposition of ink and shape retention. Deposition of only silk solution leads to frequent clogging due to shear-induced β-sheet crystallization, whereas optimized viscoelastic property of silk-gelatin blends facilitate the flow of these blends through microcapillary nozzles of varying diameter. This study demonstrates that induction of controlled changes in scaffold surface chemistry, by optimizing silk-gelatin ratio, can govern cell proliferation and maintenance of chondrocyte morphology. Microperiodic silk-gelatin scaffolds can influence postexpansion redifferentiation of goat chondrocytes by enhancing Sox-9 gene expression, aggregation, and driving cartilage matrix production, as evidenced by upregulation of collagen type II and aggrecan expression. The strategy for optimizing redifferentiation of chondrocytes can offer valuable consideration in scaffold-based cartilage repair strategies.

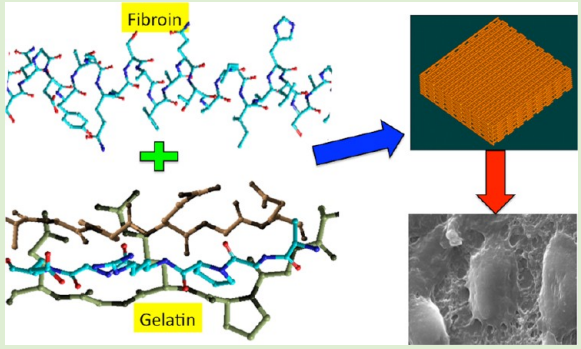

INTRODUCTION

Tissue engineering studies are moving in the direction toward personalized therapeutic strategies, where scaffolds need to be fabricated in tissue-specific, patient-specific architecture. Direct writing is one of the promising approaches to develop microperiodic complex architectured scaffolds[1,2] so as to simulate the three-dimensional (3D) microenvironments of the target tissue. Clinical images captured from the area of defect in a patient's body can be converted to virtual 3D architectures using CAD software. Using that image, the computer-controlled translation stage of direct-write assembly can move a syringe barrel incorporated with an ink deposition micronozzle in a layer-by-layer fashion, to form controlled and complex 3D constructs. Use of biopolymers for fabricating such scaffolds is advantageous, as it refrains the coarse conditions of solvents and temperature, thereby allowing the incorporation of additional bioactive components.

We have previously reported regenerated silk fibroin (SF) protein-based scaffolds by using direct-write assembly, which supported chondrogenic differentiation of human mesenchymal progenitor cells.[2] However, frequent choking of nozzles due to shear-induced β-sheet crystallization was a bottleneck to ensure reproducibility during scaffold fabrication. Furthermore, *Bombyx mori* SF protein macromolecules do not have cell adhesion motifs *per se*. In several studies an integrin-recognizing RGD peptide sequence was attached to SF protein by chemical cross-linking in order to elevate cellular attachment and proliferation.[3,4] Gelatin, the denatured form of collagen, has cell-adhesive RGD motifs, and can be used to enhance cell attachment.[5] Hence, in this study gelatin was used along with SF protein to develop a sol−gel ink for ease of scaffold fabrication, as well as to impart biofunctionalization. To the best of our knowledge, micropatterned scaffolds with silk−gelatin blend have not been reported.

Ink design is a pertinent issue for direct writing at the microscale. Rheological properties of the ink must be systematically investigated to establish correlations between composition and flowability.[6] Several reports investigated hydrogels or films comprised of silk and gelatin, either by physical mixing or chemical cross-linking. Chemical cross-linkers, such as methacrylamide, glutaraldehyde can lead to toxicity.[7,8] Interestingly, Gil et al.[9] demonstrated that physical mixing of fibroin with gelatin, followed by alcohol-based solvent casting, resulted in physically cross-linked interpenetrating

Received: July 27, 2012
Revised: January 4, 2013
Published: January 10, 2013

networks (IPNs)/semi-IPNs. Unconstrained molecular mobility was preserved in this blend, wherein the fibroin fraction could undergo conformational transition from random coil to β-sheet in the presence of aqueous alcohol solutions, and gelatin chains could undergo conformational transition from helix-to-random coil between atmospheric and body temperature. The hydrogel network was maintained by the introduction of β-sheet conformation, thereby enhancing the solid-like behavior of the hydrogels even at increased temperatures beyond body temperature.[9] As these macromolecular blends showed no sign of macroscopic phase separation before or after exposure to aqueous alcohol, these blends could be useful as ink for direct writing to develop protein-based biomaterials.

Isolation and culture of chondrocytes as a monolayer causes dramatic alteration in their differentiation profile. Upon monolayer expansion chondrocytes undergo dedifferentiation, during which they strongly express actin cytoskeleton, acquire fibroblastic spread morphology and produce collagen type I, collagen type III and versican, whereas in the differentiated state they express collagen type II and aggrecan. When cultured over appropriate scaffold matrix in 3D context, the dedifferentiated chondrocytes are able to redifferentiate and upregulate the synthesis of cartilage matrix proteins. Hence, optimization of scaffold composition is of significant clinical importance for cartilage tissue engineering. In this report, we attempted to evaluate the redifferentiation potential of goat articular chondrocytes over microperiodic scaffolds made from only silk and silk-gelatin blends. Cell adhesion and modulation in shape were investigated by scanning electron microscopy (SEM). Postexpansion redifferentiation capacity was assessed by quantification of chondrogenic gene expression using real-time polymerase chain reaction.

EXPERIMENTAL SECTION

Materials. *Bombyx mori* cocoons were kindly provided by Central Silk Technological Research Institute (Central Silk Board), Bangalore, Ministry of Textiles, Government of India. Gelatin powder (Bovine skin, Type B) was purchased from Sigma Aldrich, India.

Methods. *Preparation of SF Solution.* The master SF solution was prepared as mentioned earlier,[2,10] by cutting the silk cocoons into small pieces and boiling the pieces for 20 min in an aqueous solution of 0.02 M Na_2CO_3. This degumming process was repeated thrice, and then SF fibers were rinsed thoroughly with distilled water to remove the glue-like sericin protein. The extracted fibroin fibres were dried at room temperature. This fibroin was then dissolved in 9.3 M LiBr (Sisco Research Laboratories Pvt. Ltd., India) solution at 60 °C for 4 h, yielding a 20% w/v aqueous solution. This SF solution was dialyzed against distilled water using Slide-a-Lyzer dialysis cassette (MWCO 3500, Pierce) at room temperature for 3 days with successive water change to remove the salt. The final concentration of the SF aqueous solution was calculated to be 5% w/v. This procured 5% w/v SF solution was dialyzed against 20% poly(ethylene glycol) (PEG) (6000 g/mol, Fisher Scientific) at room temperature in order to obtain concentrated SF solution. After the required time of dialysis against PEG, 28−30 wt % of SF solution was obtained. The solution was kept at 4 °C prior to printing to avoid premature gelation.

Preparation of Silk−Gelatin Blend. Silk fibroin−gelatin (SF-G) blends were prepared by adding desired amount (5−50 wt %) of gelatin powder in 5−20% w/v SF solution, and the suspensions were kept under agitation at 40 °C. For the following studies, the percentages of the SF solutions and gelatin were varied as shown in Table 1.[11]

Rheological Measurements. The rheological properties of different concentrations of silk fibroin solutions (5−28%), gelatin (10−50%) and SF−G blends (keeping SF constant at 5 or 10 wt % and varying the gelatin concentration from 5 wt % to 50 wt %) were measured at 25 °C using Bohlin CVO Rheometer, Malvern Instruments, Malvern, UK, with a cone and plate geometry (CP 4/40, cone diameter of 40 mm with 4° angle). To evaluate the flow behavior, viscosity of these solutions was measured at different shear rates in rate-controlled mode. The environmental cuff was used in all the experiment. Care was taken during filling the geometry in order to avoid under- or overfilling. All the biopolymer solutions were evaluated for the shear rate range from 0.1 to 1000 s^{-1} by selecting 10 points in each decade. The dynamic elastic modulus (G') and viscous modulus (G'') were also measured in oscillatory mode. Linear viscoelastic region of the materials were found out from amplitude and frequency sweep measurements prior to gelation kinetic study. In the amplitude sweep measurement, the materials were tested for strain value of 0.1 to 10^4 % by keeping the frequency constant at 1 Hz, and in the frequency sweep measurement, materials were tested from 0.1 to 100 Hz frequency range by keeping the strain constant at 5% (Figure S1).

Table 1. Preparation of SF−G Blends

	weight fraction	
blends	silk fibroin (SF)	gelatin (G)
5SF-5G	5%	5%
5SF-10G	5%	10%
5SF-20G	5%	20%
5SF-30G	5%	30%
5SF-40G	5%	40%
5SF-50G	5%	50%
10SF-5G	10%	5%
10SF-10G	10%	10%
20SF-20G	20%	20%

For gelation kinetics study, the target strain value of 5% and frequency value of 1 Hz were selected from one-third of the linear region, before the crossover points of G' and G'', from amplitude sweep and frequency sweep results, respectively. The above strain amplitude and frequency were selected to ensure that the measurements were conducted within the linear viscoelastic region and that the G' and G'' were independent of the strain amplitude and frequency. To evaluate the difference in gelling behavior induced by absolute methanol and absolute ethanol, gelation kinetics of the solutions were studied with time in oscillation mode. Gel was formed by incubating the solution with coagulant for 5−10 min, and gel strength was determined with amplitude sweep measurement. Each test was carried out in triplicate, and for statistical analysis, a two-tailed Student's t test was used. Differences were considered to be significant at $p < 0.05$.

Fourier Transform Infrared Spectroscopy (FTIR). FTIR spectra of vacuum-dried silk, gelatin and SF-G mixture were obtained using FTIR spectrophotometer (Perkin-Elmer, Spectrum BX, FT-IR system, DTGS (Deuterated Triglycine Sulfate) IR detector) in transmission mode, with spectral resolution 4 cm^{-1}, number of scans 50, and then the spectra were analyzed for relative comparison. All scans were done at the same spot of the same piece of material for each sample. FTIR spectra of the samples under absorbance mode were drawn from 1200 to 1750 cm^{-1} wave numbers with an applied offset value of 0.1−0.6 (a.u.) to avoid the overlapping of the spectrum. Fourier self-deconvolution (FSD) of spectra was performed using OriginPro 8.0 (OriginLab Corporation, Northampton, MA, USA) following the method described elsewhere.[12] Fitting of the FSD FTIR spectra with Gaussian profiles was done in the amide I region between 1595 and 1705 cm^{-1} and its β-sheet fraction was determined by integral of Gaussian profiles (termed "bands"). Bands between 1617 and 1637 cm^{-1} and between 1697 and 1703 cm^{-1} indicated formation of β-sheet crystals.[13] The β-sheet fraction was reported by taking the ratio of these bands to the total amide I bands. Each test was carried out in triplicate and for statistical analysis a two-tailed Student's t test was used. Differences were considered to be significant at $p < 0.05$.

Differential Scanning Calorimetry (DSC). All SF-G blends were soaked in absolute methanol for 1 day to induce β-sheet crystallization

of SF molecules in the blends. The treated SF-G blends and the dried gelatin film were soaked in deionized water at 10 °C for 1 day to swell and were wiped with tissue paper. Five to eight milligrams of swollen hydrogels samples (n = 3) were placed in sealed aluminum pan via crimping and heated in a Perkin-Elmer DSC (Pyris 6 DSC). After 5 min of holding time at 0 °C, the samples were heated to 100 °C at the rate of 5 °C/min.

Scaffold Manufacturing. SF and SF-G microperiodic scaffolds were prepared by extruding the SF and SF-G ink through a range of microcapillary nozzles (precision microdot stainless steel tip with 90 and 60 μm diameters (Nordson, EFD, Inc., USA), or borosilicate glass microtip of inner diameter 10 μm (TIP10TW1-L), 5 μm (TIP5TW1LS01) (from World Precision Instruments, Sarasota, FL, USA)) mounted onto a three-axis, computer-controlled robotic stage (Fiber Align, Aerotech Inc., Pittsburgh) of direct-write assembly into absolute methanol drop (~250 μL) placed on siliconized glass slides (Hampton Research, CA, USA). The writing speed was 0.5 mm/sec at 17 psi pressure, which was controlled by customized software (3D Inks, Stillwater, OK, USA). As the biopolymer ink extruded out of the nozzle, continuous filament-like structures were developed due to fast and enhanced solidification by activating the β-sheet crystallization of SF component and coagulation of the gelatin portion. After one fibrous layer was developed, the nozzle was incrementally raised (e.g., 60 μm raised when the 60 μm diameter microcapillary nozzle was used) to deposit the next layer.[2] The overall dimensions of microperiodic scaffold were in the range of 4 mm^2 to 100 mm^2 in the $x-y$ plane, with 6−10 layers. Finally, scaffolds of 25 mm^2 were used for cell culture studies.

The coagulated gelatin portion in silk-gelatin blend may transform back from helix to random-coil if it is dipped in aqueous solution at 37 °C. In order to make the scaffolds stable during cell culture at 37 °C, the SF-G scaffolds were cross-linked with 1-ethyl-3,3-dimethyl aminopropyl-carbodiimide (EDC)−*N*-hydroxysuccinimide (NHS) using 12.0 mM EDC and 4.8 mM NHS for 3 h at room temperature.[14] An unstable reactive *o*-acylisourea ester is formed as soon as EDC reacts with the carboxyl group present in the protein. The NHS reacts with this unstable ester to form a semistable NHS ester, which in turn reacts with amine group of another protein and gives rise to stable peptide bonds, thereby extricating EDC and NHS. The pH of the solution was maintained at 5.5 (monitored by using an electronic pH meter) during cross-linking, and changes (if any) were adjusted by dropwise addition of either 1 M NaOH or HCl. The remaining NHS activated carboxylic acid groups were hydrolyzed by washing the cross-linked samples thoroughly for 2 h with 0.1 M Na_2HPO_4. Subsequently, the microperiodic scaffolds were washed three times with distilled water and dried at room temperature.

Cell Culture. Chondrocytes were isolated from goat articular cartilage by enzymatic digestion using 0.1% collagenase type II (Gibco) for 24 h, washed with phosphate buffered saline without calcium or magnesium and pH 7.4 (Lonza). The digest was filtered through 70 μm mesh, and the single cell suspension was seeded for expansion at a density of 6000 cells/cm^2 with Dulbecco's modified Eagle's medium (Cellclone) supplemented with 10% fetal bovine serum (Biological Industries), 1% penicillin/streptomycin, 2.5 μg of Amphotericin B, 5 ng/mL of FGF-2 (Millipore) and 2 ng/mL of TGFβ 1 (Millipore). To investigate the effect of scaffold chemistry on cell behavior (morphology, spreading and gene expression profile), the expanded goat chondrocytes (P1) were seeded at a density of 10^5 cells/cm^2 on the SF (24% w/v) and 5SF-30G scaffolds and cultured for 28 days in the presence of TGFβ 1 containing media.

Scanning Electron Microscope (SEM). The samples were vacuum-dried and then coated with gold using a gold sputter coater (EMITECH K550X, UK) for 1 min with 25 mAmp electric current, to form 15−20 nm thickness of coating. Microperiodic morphology of the scaffolds was observed using an SEM (Model EVO 50, Zeiss, UK) under vacuum. Cellular morphology was assessed by selecting at least 25 cells from different locations on the scaffold. Images were captured at different magnification for determination of cell morphology, cell attachment, cell surface area, and cell extensions such as filopodia and lamellipodia, and quantified using NIH Image J software.

Quantitative Real-Time Polymerase Chain Reaction (RT-PCR). Total messenger RNA (mRNA) was isolated from engineered constructs using an Rneasy mini kit (Qiagen). RNA concentration and the purity was determined using a Nanodrop spectrophotometer (Thermo Scientific). Extracted RNA were reverse-transcribed into cDNA using first strand cDNA Synthesis Kit (Fermentas). Quantitative real-time RT-PCR was conducted using SYBR Green Master Mix and Rotor gene Q thermocycler (Qiagen). The reactions were carried out in duplicate in 25 μL total volume containing 1 μL cDNA and 2.5 μL primer. The Assay on demand (Qiagen) primers used were GAPDH (Cat No: QT00079247), RhoA (Cat No: QT00044723), Rac1 (Cat No: QT00065856), Collagen I (Cat No: QT00037793), Collagen II (Cat No: QT00049518), Sox-9 (Cat No: QT00001498), Aggrecan (Cat No: QT00001365). The analysis was carried out with the Rotor gene Q software and the relative expression levels were calculated using the $2^{-(\Delta\Delta c(t))}$ method with GAPDH as a control. For each time point, samples of silk and silk-gelatin in duplicates were analyzed. Statistical analyses were carried out using Mann−Whitney test with $p \leq 0.05$ as the criterion for statistical significance.

RESULTS AND DISCUSSION

The main objective of this study was to develop a microperiodic 3D scaffold, by ensuring smooth flow and fast solidification of ink and functionalized surface composition that would facilitate redifferentiation of chondrocytes. Polymer ink to be used for direct writing must satisfy following criteria.[2] First, the rheological features of ink should ensure smooth extrusion through the fine diameter micronozzle under high shear rates (~20−200 s^{-1}), without any choking or fracture. Second, the ink should have tailored viscoelasticity, so that it can be extruded uniformly through the nozzle under the applied pressure and should change from fluid-like phase to solid-like phase soon after emerging from the nozzle maintaining cylindrical filamentary shape to ensure shape retention. So the viscous modulus of the ink should be higher than the elastic modulus prior to extrusion. After extrusion, the coagulation solvent should be able to transform the ink into gel with sufficiently higher modulus of elasticity to ease writing and retention of the uniform filament diameter. Third, once deposited it should become self-supporting during spanning gaps on the underlying layers as a result of solvent assisted solidification. Hence, after extrusion the ink should have its elastic modulus higher than the viscous modulus ($G' \geq G''$). It should be noted that, the shear thinning behavior of the ink also promotes easy solidification due to significant increase in viscosity as the shear rate reduces to zero soon after injecting. Precise optimization of these constellations of parameters would open up new avenues for developing 3D architectures for a broad array of applications.[15−17]

Rheological Characterization. SF solutions displayed shear rate-dependent viscosity behavior (shear thinning) at low concentrations (<20 wt %), and beyond this critical concentration it appeared more like a Newtonian fluid with less dependence on shear rate, as reported earlier.[2] Shear thinning behavior can be explained by the alignment of physically entangled fibroin chains due to the applied shear stress at lower concentration of silk. By contrast, at higher concentrations mobility of macromolecular chains is suppressed, hindering their capacity to self-organize into an assembled aligned structure. Interestingly, 28% silk solution showed sharp shear thickening behavior at shear rate above 100 s^{-1} (Figure 1a), due to shear induced β-sheet crystallization,[18,19] which might be the main cause of choking of micronozzles during direct writing. Most of the rheology studies on highly concentrated silk

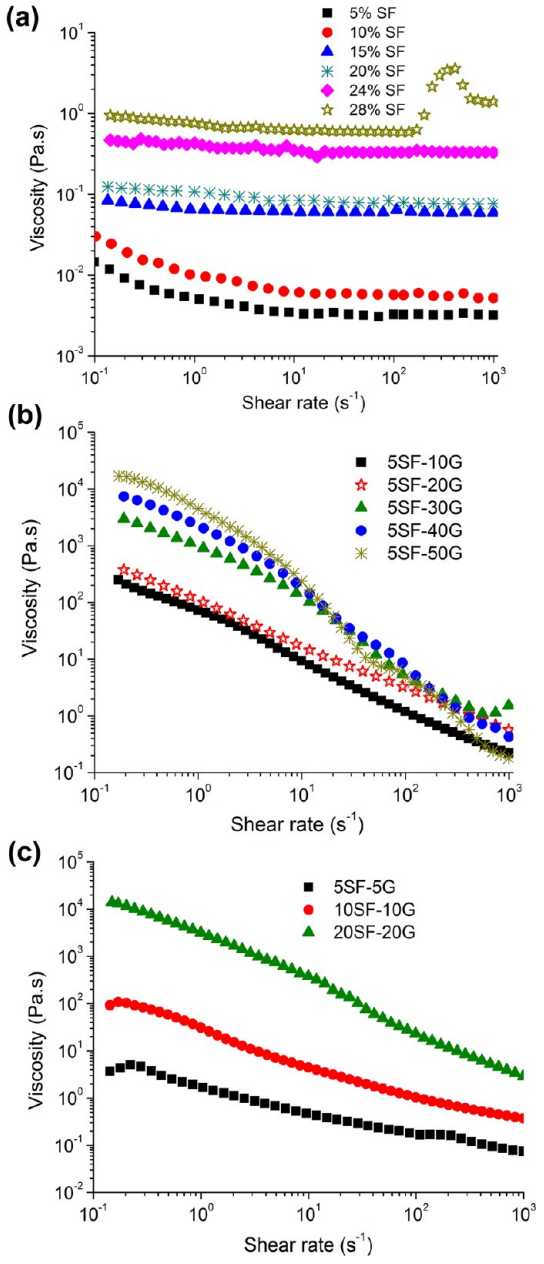

Figure 1. (a) Viscosity of SF solution at various concentrations. (b) Viscosity of SF-G blends of different ratio. (c) Viscosity of SF-G blends of same ratio at varying shear rate.

solution[2,9,12] were conducted up to shear rate of 100 s^{-1}; hence, the shear thickening behavior as highlighted in this study was not elucidated in the literature. When higher concentrated silk solution is subjected to large shear force (>100 s^{-1}) thermodynamic, as well as kinetic processes drive transition of random coil to β-sheet conformation resulting in shear thickening behavior.[2,19,20] This concept was further corroborated by the observation of deposition of whitish semisolid aggregates immediately after the rheological test under high shear rate.

Interestingly, SF-G blends at wide concentration range showed shear thinning behavior (Figure 1b,c), mainly due to the formation of an interpenetrating gel network through physical cross-linking. The shear thinning behavior of gelatin (data not shown) may also be responsible for this property of blends at all compositions, as the effect was more pronounced with higher ratio of gelatin in the blend. Moreover, differences in isoelectric point of silk and gelatin could be another factor for inducing this physical gel formation. The isoelectric point of silk is lower than 7, while that of gelatin is greater than 7. Under physiological conditions (pH 7.2−7.4), these two biomacromolecules have opposite charges, which could yield suitable binding.[21] This gelation behavior would be crucial for direct writing to facilitate smooth flow of polymer ink through the nozzle and produce self-supportive patterned filaments.[22] The viscosities of 28% SF solution and 5SF-50G and 20SF-20G blends were 0.59 ± 0.03, 4.87 ± 0.21 and 23 ± 0.72 Pa·s, respectively, at 100 s^{-1} shear rate. The volumetric flow rate of the ink through 90 μm diameter microcapillary needle under the applied pneumatic pressure (13−28 psi) was approximately 1−1.7 × 10^{-11} m^3/s. So, the applied shear rate was approximately 139.79−59.41 s^{-1}. Thus, the viscosity of SF solution and SF-G blends was reported at 100 s^{-1} shear rate. It is interesting to note that although 5SF-50G contains highest polymer loading (polymer loading 55%), viscosity of 5SF-40G (polymer loading 45%; 8.67 ± 0.25 Pa·s) was higher than that of 5SF-50G (4.87 ± 0.21 Pa·s) at 100 s^{-1}. Further, the viscosity of 20SF-20G (23 ± 0.72 Pa·s) was ∼23 times higher than that of 10SF-10G (1.04 ± 0.02 Pa·s) and viscosity of 10SF-10G was ∼10 times higher than that of 5SF-5G (0.16 ± 0.01 Pa·s) at 100 s^{-1} shear rate, however, the polymer loading of 20SF-20G (polymer loading 40%) and 10SF-10G (polymer loading 20%) is just double than that of 10SF-10G and 5SF-5G (polymer loading 10%), respectively. Thus, the viscosity of the SF-G blends is not only due to the effect of total amount of biopolymer present. Interaction between two oppositely charged polymers in the blends results in enhanced viscosities for higher polymer loaded blends, which is very much prominent in 5SF-40G and 20SF-20G blends.

Blend optimization was done through viscoelastic measurement of SF-G blends at different ratio under oscillatory mode. The elastic and viscous moduli of 28% SF solution were 1.4 and 6.75 Pa, respectively (Figure 2a). Mixing of gelatin to the SF caused dramatic increase of elastic behavior of the SF-G blends. The elastic modulus and viscous modulus of 5SF-50G blend were 3020 ± 154.78 Pa and 670 ± 34.86 Pa, respectively, under oscillation at 1% strain and constant frequency of 1 Hz (Figure 2b). It is important to mention that, except 5SF-10G, all other SF-G blends revealed more solid-like behavior at 1 Hz, as shown by the higher elastic modulus than the viscous modulus below 100% strain. Higher gelatin containing (5SF-50G and 5SF-40G) blends showed very high elastic modulus (>2000 Pa), which prevented their flow through the microneedle during direct writing. However, the lower gelatin containing SF-G blends (5SF-30G and 5SF-20G), having lower elastic modulus (<2000 Pa), allowed smooth flow through the microneedle under applied pneumatic pressure. So, 5SF-30G and 5SF-20G blends were found to be optimal for preparation of microperiodic structure via direct-write assembly.

In the case of same-ratio SF-G blends, the elastic modulus was higher than the viscous modulus for 20SF-20G below 100% strain (Figure 2c). For other samples (5SF-5G and 10SF-10G), viscous modulus was higher than the elastic modulus, exhibiting a more liquid-like response (Table 2). Hence, among same ratio SF-G blends, 20SF-20G was found to be suitable for preparation of microperiodic structure via direct-write assembly.

To evaluate the gelation kinetics of different blends, studies were carried out in either absolute methanol or ethanol as

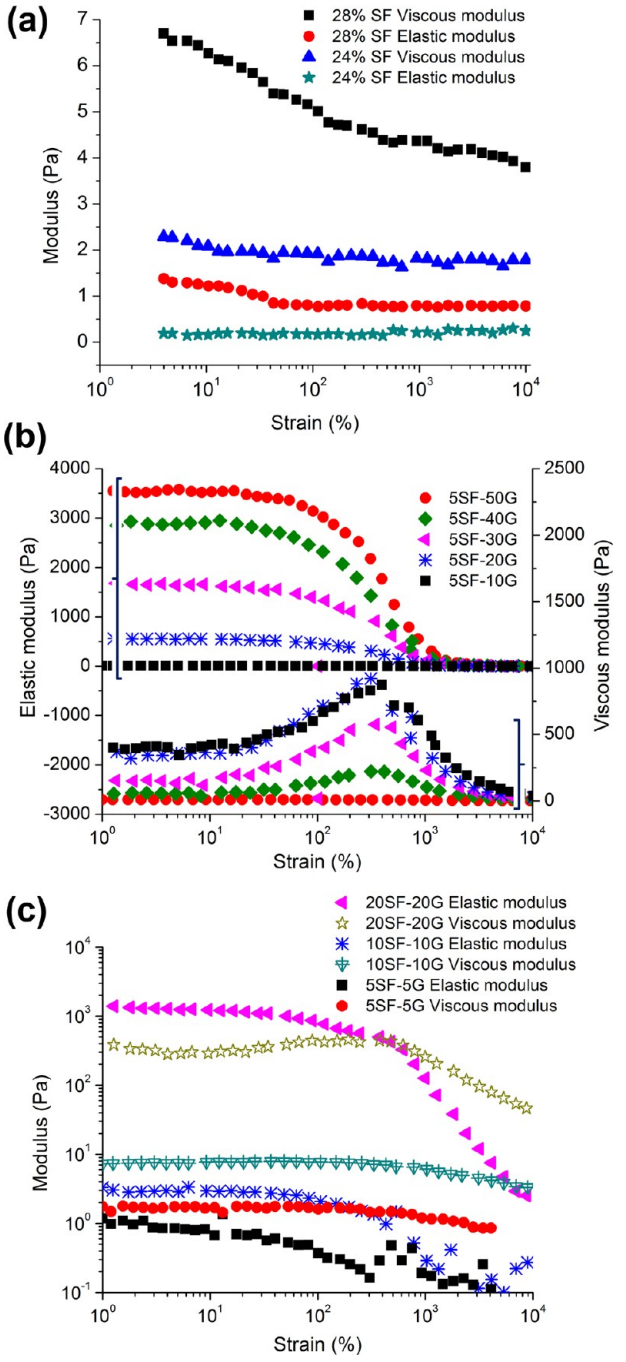

Figure 2. (a) Elastic and viscous modulus of SF. (b) Elastic and viscous modulus of SF-G blends of different ratio. (c) Elastic and viscous modulus of SF-G blends of same ratio.

coagulation bath, at 25 °C under oscillatory mode by time sweep measurement at constant strain value of 5% and frequency value of 1 Hz. The measurement was carried out at isothermal condition as β-sheet crystallization of silk molecules upon exposure to alcohol and subsequent entanglement with gelatin molecules expected to form physical gel.[9,12] SF-G blends exhibited a fluid-to-gel transition upon alcohol exposure (Figure 3). Before coming in contact with coagulant, the system resided in the linear viscoelastic region and complex viscosity (η^*) was independent of time, but after exposure to the coagulant, complex viscosity of the system increased many fold with time due to transformation from random-coil to β-sheet crystallization of the SF resulting an increase in stiffness of the gel. Both the shear yield stress and elastic modulus increased by several orders of magnitude because of crystallization and solidification (dehydration).

Interestingly, 5SF-10G showed a sharp and significant increase in η^* among others (Figure 3c,d). This may be due to the fact that lower weight fraction of gelatin in SF-G gels facilitated diffusion of methanol or ethanol through the loosely placed macromolecules, whereas, in case of higher weight fraction gelatin in SF-G gels, the gelatin macromolecular chains were densely arranged which reduced the diffusion rate of alcohol from surface to core of the gel. It was also observed that the gelation kinetics was faster in case of methanol than that of ethanol (Figure 3a,b). This may be due to fact that methanol can penetrate faster through the densely arranged macromolecular chains of the polymer solution as the viscosity of absolute methanol (5.44×10^{-4} Pa·s) at 25 °C is close to half of that of absolute ethanol (1.074×10^{-3} Pa·s).[23] Hence, methanol has higher dehydrating ability than that of ethanol. Interestingly, magnitude of η^* of SF gel coagulated by methanol was approximately 1.5 times higher than that of SF gel coagulated by ethanol. The same was also been observed in the case of SF-G blends with higher weight fraction of gelatin. Hence, finally methanol was used as coagulant to prepare SF and SF-G microperiodic structures through direct-write assembly in the present study.

FTIR Analysis. FTIR was used to evaluate the conformation of the SF protein in the blend after absolute methanol treatment. The absorbance data for methanol-treated dried SF-G blends are shown in Figure 4a, depicting the absorption bands for amide I, amide II, and amide III at 1624, 1516, and 1265 cm^{-1} respectively, confirming the presence of β-sheet structure.[24,25]

To ascertain whether the presence of gelatin could influence solvent-induced SF crystallization by physical hindrance offered by the entangled SF and G biomacromolecules, we investigated the FTIR signature of SF-G blends. When blended polymers are thermodynamically compatible and chemical moieties

Table 2. Weight Ratio of the Polymer Blends and Their Rheological Properties

samples	dry weight of SF (%)	dry weight of gelatin (%)	total dry weight of polymer (%)	viscosity at 100 s^{-1} shear rate (Pa·s) (mean ± SD)	elastic modulus at 1% strain (Pa) (mean ± SD)	viscous modulus at 1% strain (Pa) (mean ± SD)
5SF-10G	5	10	15	1.19 ± 0.03	7.71 ± 0.42	9.39 ± 0.38
5SF-20G	5	20	25	3.3 ± 0.08	448 ± 12.58	145 ± 2.85
5SF-30G	5	30	35	5.43 ± 0.12	1330 ± 98.24	402 ± 13.49
5SF-40G	5	40	45	8.67 ± 0.25	2320 ± 120.58	714 ± 41.91
5SF-50G	5	50	55	4.87 ± 0.21	3020 ± 154.78	670 ± 34.86
5SF-5G	5	5	10	0.167 ± 0.01	0.371 ± 0.008	1.6 ± 0.04
10SF-10G	10	10	20	1.04 ± 0.02	2.07 ± 0.07	7.71 ± 0.54
20SF-20G	20	20	40	23 ± 0.72	766 ± 49.42	423 ± 19.58

dx.doi.org/10.1021/bm301193t | *Biomacromolecules* 2013, 14, 311−321

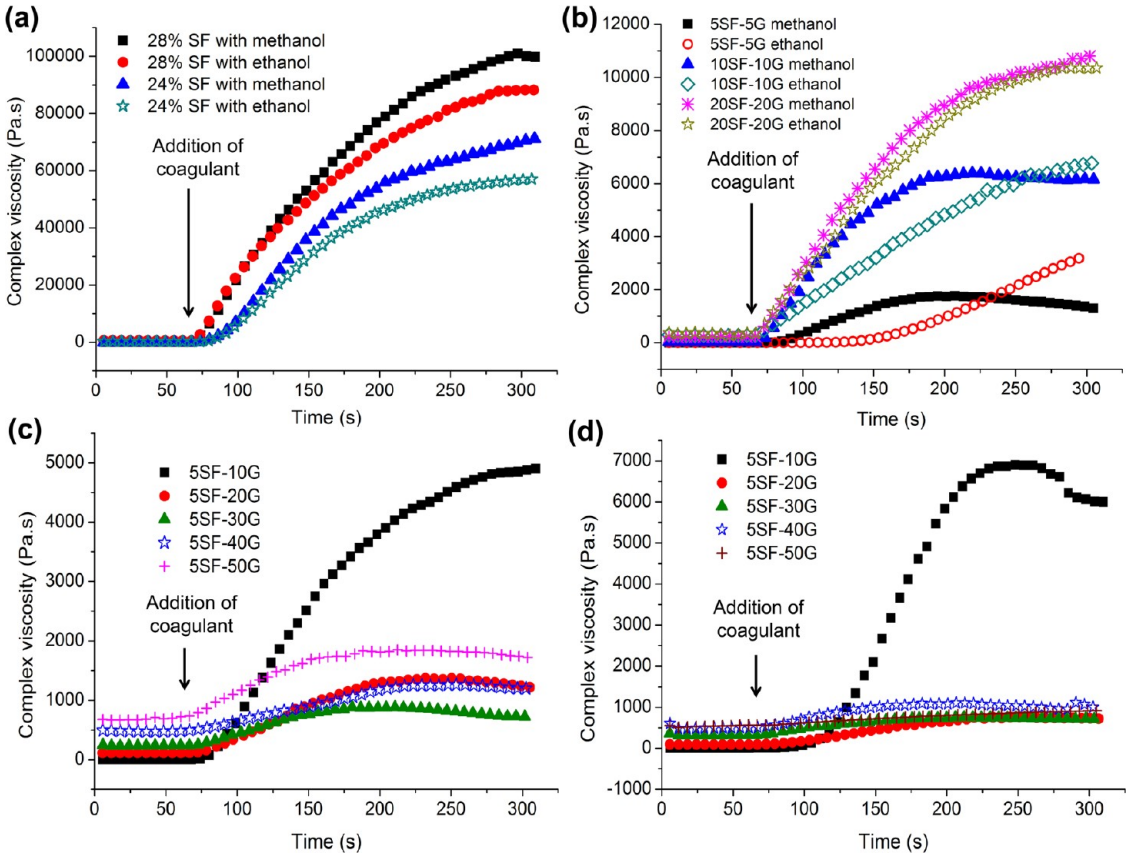

Figure 3. (a) Gelation kinetics of SF with methanol and ethanol. (b) Gelation kinetics of SF-G blends of same ratio with both methanol and ethanol. (c) Gelation kinetics of SF-G blends of varied ratio with methanol. (d) Gelation kinetics of SF-G blends of varied ratio with ethanol.

facilitate intermolecular interactions between them, the resultant FTIR spectra of the blended composition differs from those of the constituent polymers.[9] Conversely, blends of two incompatible (phase-separated) polymers yield FTIR spectra in which the spectra of the two polymers are superimposed.[9] Gil et al.[26] previously reported that these two proteins prior to methanol treatment were compatible and intermingle to form supramolecular organization. In our study, all the blends treated with absolute methanol showed the absorption bands correlating with the β-sheet conformation of SF: 1628 cm^{-1} (amide I), 1530 cm^{-1} (amide II), and 1267 cm^{-1} (amide III).[12,27] These results were comparable to those obtained from pure SF (Figure 4a). This finding confirmed that the presence of gelatin could not constrain the molecular mobility required during reorganization of SF polymer chains from random-coil to β-sheet conformation during methanol-induced transformation.

The secondary structure of SF-G blends formed after methanol treatment was further elucidated by deconvolution of the IR spectra[27] (Figure 4b). The relative ratios of β-sheet fraction was calculated from the amide I region of SF-G blends by using FSD analysis (Figure 4c). The β-sheet content of pure SF was 41.7%, which was similar to the % fraction reported by others.[28] However, addition of gelatin to the SF first resulted in slight reduction and then enhancement in the β-sheet content of SF-G blends. The β-sheet contents of SF-G blends were 30.4, 27.9, 28.2, 35.1, and 30.5% for 5SF-10G, 5SF-20G, 5SF-30G, 5SF-40G, and 5SF-50G, respectively. There was a significant difference in β-sheet content between 5SF-10G and 5SF-40G (p = 0.048). Further, as gelatin content increased from 5% to 10%, β-sheet content increased from 32.9% to 36.9% in 10SF-5G to 10SF-10G respectively (p = 0.01). From the results it can be postulated that as the weight fraction of gelatin increases in the blend, the β-sheet fraction also increases. One possible reason for this can be the accessibility of methanol by the SF chains in the blends. It has been reported that gelatin facilitates diffusion of methanol in the SF-G blends, while the crystallized β-sheet restricts its diffusion.[12] Thus, the transformation of random coil to β-sheet crystallization was more in the case of higher gelatin weight fraction.

DSC Analysis. DSC heating curves of gelatin and SF-G blends are shown in Figure 5. Herein, we investigate the capacity of methanol induced β-sheet networks to modify the transition temperature of gelatin in SF-G blend. The molecular conformation of SF changes the transition temperature of gelatin in the SF-G blend.[12] The SF-G blends were treated with absolute methanol at 10 °C so as to induce β-sheet crystallization of SF molecules in the presence of the triple helix structure of gelatin. The prepared gelatin and SF-G films were swollen in deionized water at 10 °C for 1 day. These swollen hydrogels displayed endothermic peaks correlating with the helix−coil transition (resulting in gel−sol transition) of gelatin.[12]

As seen in Table 3, the transition temperature increased from gelatin, 5SF-10G to 5SF-30G and then decreased in 5SF-50G. The transition temperatures of pure gelatin and 5SF-50G were nearly similar. Reduction of temperature in the trend from 5SF-30G to 5SF-50G and pure gelatin could be due to the water content in the blends that acts as a dispersant to shift the

dx.doi.org/10.1021/bm301193t | *Biomacromolecules* 2013, 14, 311−321

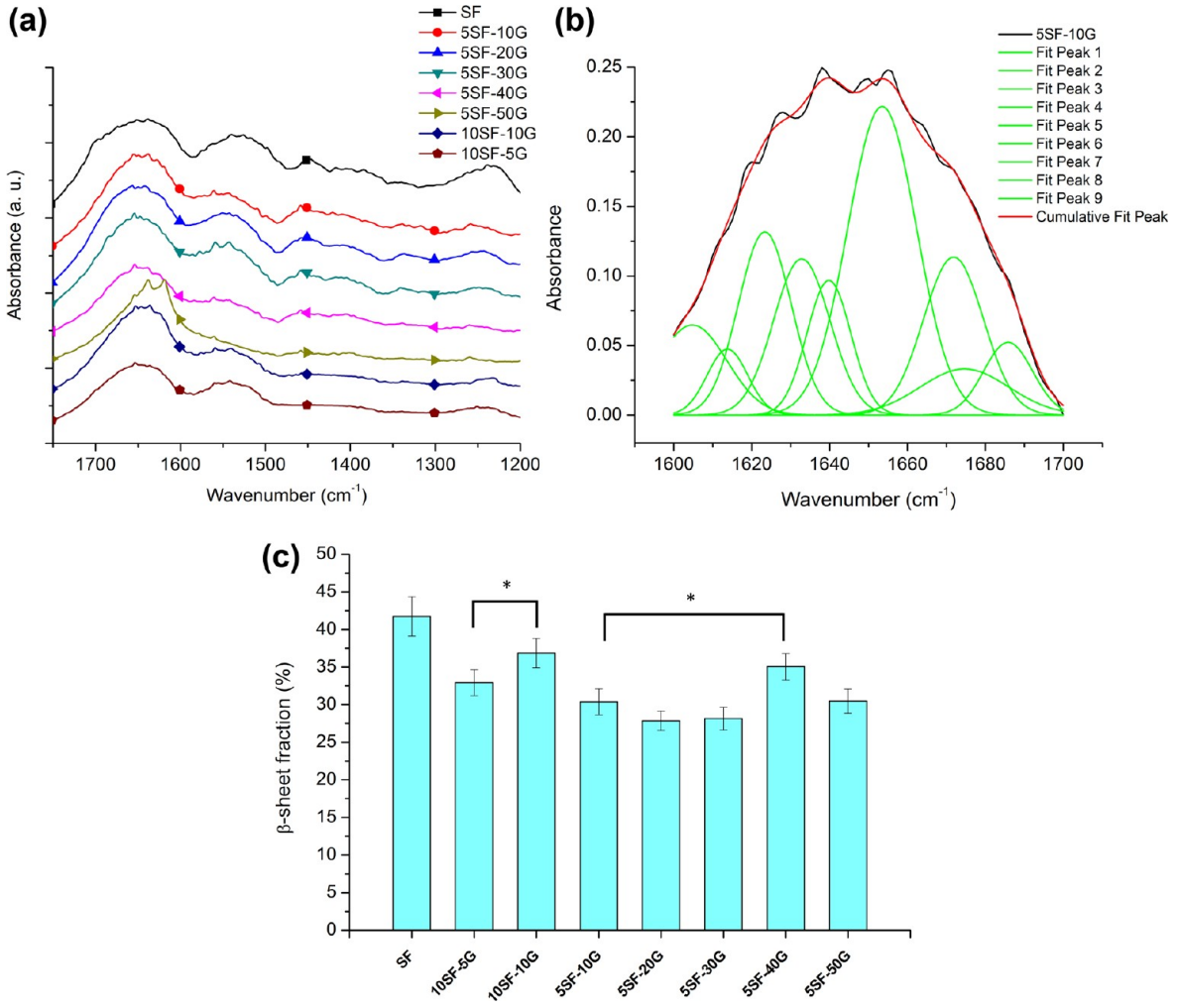

Figure 4. (a) FTIR spectra of methanol-treated SF-G blends. (b) Representative deconvoluted spectra of 5SF-10G blend. (c) β-sheet content of methanol-treated SF-G blends of varying ratios, with respect to only silk (*statistically significant difference, $p < 0.05$).

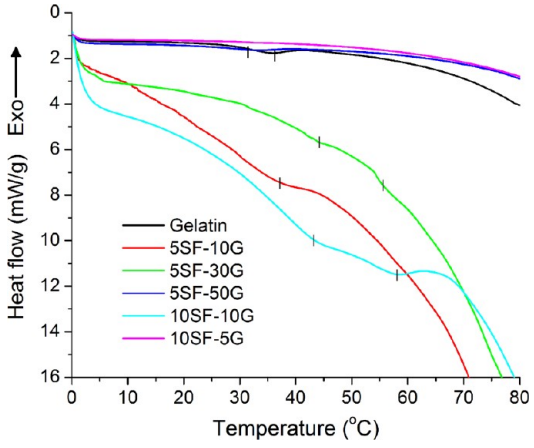

Figure 5. DSC curves of the methanol-treated gelatin and silk–gelatin blends.

transition peaks.[25] Thus, the more the gelatin percentage in the SF-G blends, the more water they contain. However, in the DSC curve of the SF-rich complex hydrogel (10SF-5G), the endothermic peak for the triple helix–coil transition was not detected in the case of gelatin. It might be because of the tight SF β-sheet networks that had completely encapsulated the

Table 3. DSC Heating Data of Gelatin and SF-G Complex Hydrogels

samples	onset temperature (°C)	peak (°C)
gelatin	28.5	35.5
5SF-10G	30.4	37
5SF-30G	33.5	42.5
5SF-50G	27.5	33.5
10SF-10G	35.3	44.9
10SF-5G		

smaller gelatin content, creating a shield and blocking the water molecules penetrating the 10SF-5G blend. Interestingly, the 10SF-10G blend exhibited different transition behaviors, compared with gelatin and other blended hydrogels (5SF-10G, 5SF-30G, 5SF-50G). Gelatin, 5SF-10G, 5SF-30G, and 5SF-50G hydrogels showed their onset temperatures at around 27.5–33.5 °C and their peak temperatures at around 33.5–42.5 °C, while 10SF-10G showed onset temperature at 35.36 °C and its peak temperature at 44.9 °C. This again could be due to the tight SF β-sheet networks. Gil et al.[26] also reported a similar shift in transition temperature in the case of SF-G blends with lower or similar gelatin weight fraction. Generally in gelatin, switching of the helix–coil transition temperature to elevated temperature takes place when it is chemically modified or cross-

dx.doi.org/10.1021/bm301193t | Biomacromolecules 2013, 14, 311–321

linked. The reason behind this temperature transition is the decrease in bound water and the existence of covalent cross-links.[11] However, in this DSC study, the prepared SF-G blends have not been chemically cross-linked. Since covalent cross-links have not been introduced in SF-G blends, this switching of helix−coil transition to elevated temperature might arise from a decrease in bound water and be due to the inhibition of tight SF β-sheet networks. Hence, these results indicate that methanol-induced β-sheet crystallized SF network in the SF-G complex can affect the helix−coil rearrangement of gelatin chains in the blend, changing the transition temperature of gelatin and potentially making it an interesting temperature-responsive IPN/semi-IPN for biomedical applications.

Scaffold Manufacturing. Addition of gelatin enabled us to prepare scaffolds of capillary size as low as in the 5 μm range, to build complex 3D layered architectures. However, in this study, only 24% w/v SF and 5SF-30G ink was chosen (based on the rheological parameter and ease of extrusion), to prepare scaffolds using a 90 μm diameter needle tip for cell culture. In order to achieve pore geometry appropriate for cellular growth and proliferation, the center-to-center spacing in the x−y plane was maintained at 200 μm. Morphological analysis of the SF and 5SF-30G filaments revealed that silk filaments had a rough surface, whereas SF-G filaments had a smooth surface (Figure 6a,b). Representative 3D microperiodic patterns generated via the direct-write technique are shown in Figure 6c−e.

Morphological Analysis of Cells. Chondrocytes adhered and proliferated robustly on both SF and 5SF-30G scaffolds.

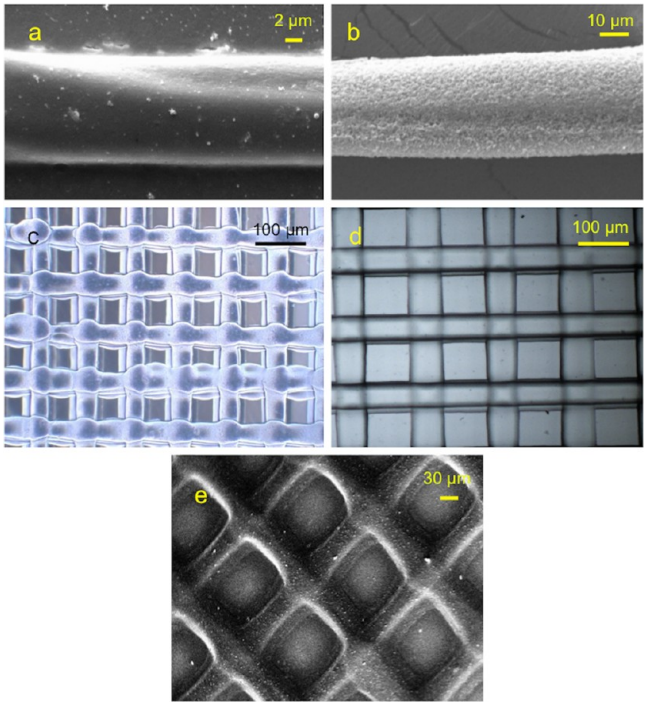

Figure 6. Direct-write scaffold self-supporting microperiodic arrays. (a,b) Magnified images of silk and silk−gelatin filaments, where the silk−gelatin blended filament (a) showed a smooth surface, but only the silk filament (b) showed a rough surface. (c,d) Representative 3D architectures of silk and silk−gelatin scaffolds, showing nonuniformity in filament diameter due to shear-induced β-sheet crystallization in only the silk scaffold, whereas silk−gelatin structures possess smooth surfaces, (e) SEM images of silk−gelatin architectures.

However, more cells could be noticed on 5SF-30G scaffolds, compared to only silk scaffold. After 2 weeks, cells achieved near-confluency on 5SF-30G scaffolds, but not on silk scaffolds. Cell morphology was spread on the silk scaffold (Figure 7a−d),

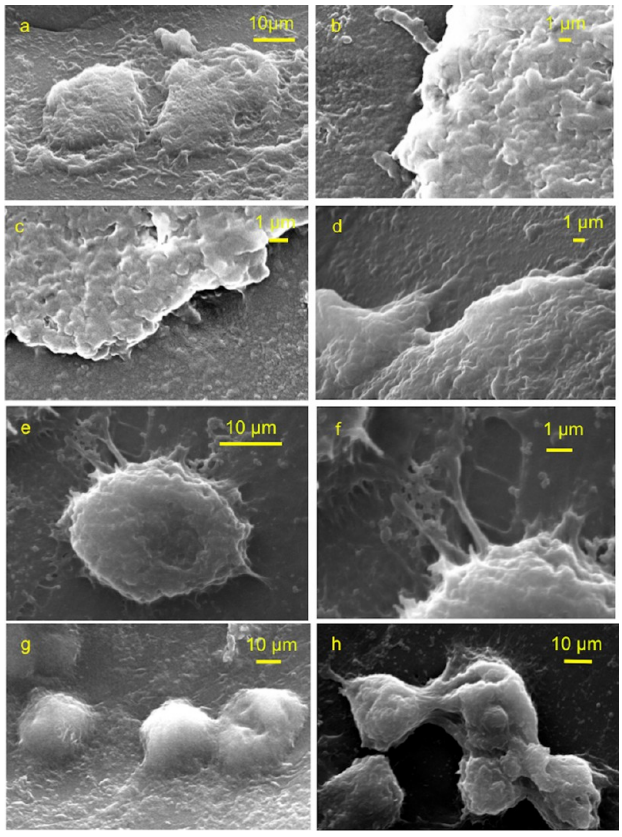

Figure 7. Cellular morphology on scaffolds. (a) Chondrocyte assumed spread morphology on a silk scaffold. (b−d) Higher magnification showing membrane ruffling of chondrocytes on a silk scaffold. (e) Rounded morphology of chondrocytes on a silk−gelatin scaffold after day 14. (f) Higher magnification showing extensive expression of filopodia from the periphery of chondrocytes on the silk−gelatin scaffold, indicating enhanced adhesion to the underlying matrix. (g) Prominent round nucleus on the silk−gelatin scaffold. (h) Aggregating chondrocytes were frequently noticed on the silk−gelatin scaffold.

probably indicating dedifferentiated state, with nominal expression of lamellipodia. However, on the 5SF-30G scaffold, cells exhibited rounded shape (Figure 7e−h) with prominent curvature of the nucleus (Figure 7g), indicating redifferentiation and maintenance of the chondrocytic phenotype and occasional extended pseudopodia or filopodia anchoring neighboring cells or matrix. Cell surface area on the SF matrix was 138.54 ± 76.745 um^2, whereas in the 5SF-30G construct it was 88.96 ± 33.12 um^2. Unlike SF (Figure 7c,d), we observed prominent cell adhesion and cell-substrate interaction in the case of 5SF-30G with many filopodial extensions (Figure 7f). Interestingly, more aggregating cells were noticed on 5SF-30G scaffold compared to the silk-only scaffold (Figure 7h).

Analysis of mRNA Transcript Expression by RT-PCR. To understand the difference in redifferentiation potential with respect to the underlying matrix composition, the transcription of cartilage specific genes in SF and 5SF-30G constructs were evaluated by RT-PCR. The transcription factor Sox-9 plays a major role in the redifferentiation process and cartilage-specific ECM protein synthesis.[29] Monolayer culture of chondrocytes is

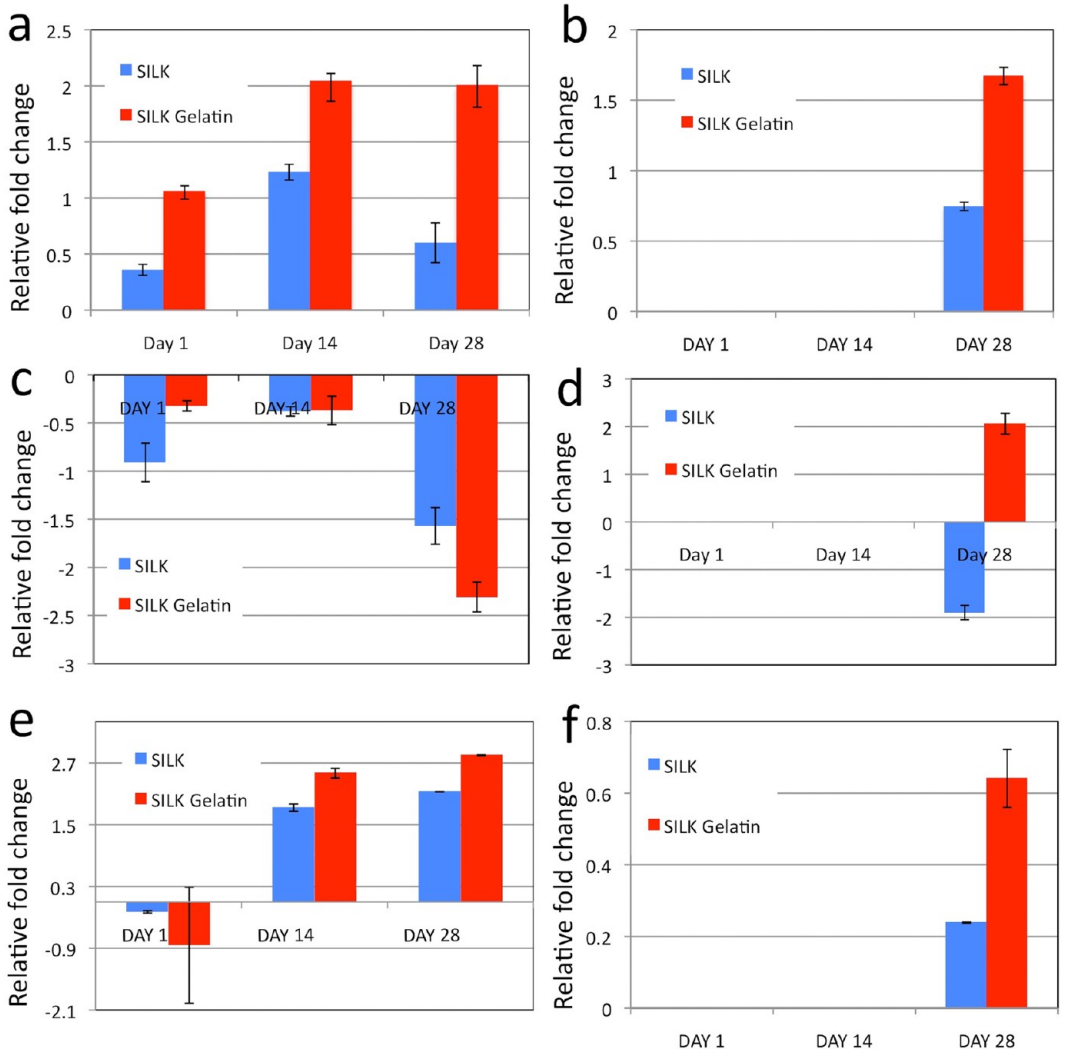

Figure 8. Gene expression analysis by RT-PCR: (a) RhoA, (b) RAC1, (c) collagen I, (d) collagen II, (e) Sox 9, (f) aggrecan. Data expressed as relative fold change for specific gene expression in silk- and silk−gelatin-based constructs at the time point mentioned.

associated with gradual loss of Sox-9, causing modulation in chondrocyte phenotype. The RT-PCR analysis indicated that the Sox-9 transcription level was downregulated on day 1 in both SF and 5SF-30G constructs and upregulated progressively with culture time (Figure 8). There was statistically significant difference ($p \leq 0.05$) between fold change level of the Sox-9 gene expression between 2 weeks and 4 weeks cultured constructs. The greater extent of upregulation of Sox-9 in the 5SF-30G construct after 2 weeks and 4 weeks of culture indicated that a higher extent of signaling cascade was activated during the redifferentiation of chondrocytes over the 5SF-30G construct than the SF-only construct.

In SF and 5SF-30G constructs, collagen I was downregulated at all time points. In the case of SF, the downregulation level was more on day 1, enhanced by 3-fold in 2 weeks, but further downregulated by 2.5-fold in 4 weeks. In comparison, the 5SF-30G constructs showed a consistent level of downregulation at two early time points, with 5-fold downregulation in the fourth week. No expression of collagen type II was detectable in either samples at two early time points. On the fourth week, in the 5SF-30G group, the collagen II gene transcription level was 2-fold upregulated, whereas, in the SF constructs, the collagen II gene expression was downregulated. Further, quantitative analysis of type II and type I collagen mRNA expression in chondrocytes after 4 weeks of culture revealed the highest collagen II:collagen I mRNA ratio for cells cultured on a 5SF-30G scaffold, compared to an SF-only scaffold, which confirmed the greater extent of redifferentiation in 5SF-30G constructs, corroborating with the flattened cellular morphology on SF and rounded morphology on the 5SF-30G scaffold.

Similarly, no expression of aggrecan (ACAN) was observed at the first two early time points. Interestingly, ACAN mRNA expression exhibited upregulation on the fourth week in both SF and 5SF-30G constructs. However, as compared to SF, 5SF-30G constructs showed 3-fold upregulation in ACAN. ACAN is a marker for chondrogenic redifferentiation, and, being a major structural component of cartilage, it plays an important role in maintaining cartilage structure and function.[30] Hence, the results suggested that culture on a 5SF-30G scaffold could enhance the redifferentiation potential of expanded chondrocytes after 4 weeks of culture.

Another important aspect of this study was modulation in cell morphology and adhesion between two matrices. Rho GTPase family members, such as RhoA, Rac1, and Cdc42 proteins, govern the morphological features and function of chondrocytes during dedifferentiation and redifferentiation.

dx.doi.org/10.1021/bm301193t | *Biomacromolecules* 2013, 14, 311−321

RhoA controls the assembly of actin stress fiber/myosin filaments to induce contractile forces,[31] while Rac1 and Cdc42 enhance polymerization of actin fibres at the periphery of the cell to generate protrusive forces by stimulating membrane ruffling and lamellipodia and filopodia formation, respectively. RhoA overexpression was found to increase proliferation and proteoglycan production, and to suppress maturation and hypertrophy.[32] Rac1 signaling is a pivotal signaling pathway for chondrogenesis to establish *N*-cadherin-dependent cellular junctions during cellular aggregation.[33]

The expression of RhoA was upregulated in both SF and 5SF-30G constructs at all the time points. In the case of silk constructs, RhoA expression increased in 2 weeks by 3.5-fold and then decreased in the fourth week. Meanwhile, in the case of 5SF-30G constructs, there was a 2-fold increase by 2 weeks that remained almost constant until the fourth week. This trend has not been observed in the case of Rac1, as there was no expression of Rac1 until the second week. Only by the fourth week was an upregulated expression of Rac1 observed in 5SF-30G constructs (2.2-fold increase) as compared to SF. Taken together, compared to the SF-only scaffold, 5SF-30G microperiodic scaffolds showed enhanced regulation of transcription of the chondrocyte-specific genes. Regulation of RhoA/Rac1 cross-talk by underlying substrate and concomitant upregulation of collagen type II expression validated observation of cellular aggregation on 5SF-30G microperiodic scaffolds. This finding is crucial for developing matrix-based cartilage tissue engineering. In our previous study[2] we concluded that a direct-write SF scaffold alone *per se* was not able to drive chondrogenic matrix production. However, in the presence of exogenous chondrogenic stimulus TGFβ, microperiodic silk architectures supported chondrogenic differentiation. The present study highlights the importance of silk-gelatin composition, along with the microperiodic 3D architecture, to support and further enhance postexpansion chondrogenic redifferentiation by modulating cell shape and upregulating chondrogenic gene expression.

Future studies are necessary to further investigate the role of differential protein adsorption on silk and silk−gelatin scaffolds, incorporation of bioactive molecules in the biopolymer system, along with the effect of spatial features of the microperiodic architecture, which might be responsible for the difference in cell−substrate interaction, the effect on cell signaling, and redifferentiation pathways.

CONCLUSIONS

Proper selection of ink composition and rheological behavior are crucial for scaffold manufacturing by the direct-write technique. Compared with silk scaffolds, modular ink composition made up of silk-gelatin blended ink could flow through the nozzle without clogging facilitating scaffold manufacturing. This study highlights the need to select proper surface composition of the biomaterial to modulate the gene expression profile. SF-G blended hydrogel scaffolds supported redifferentiation of chondrocytes and maintained chondrocyte phenotype better than a silk-only scaffold. Development of microperiodic scaffold with tailor-made architectural features has the potential to greatly facilitate the biomaterial-based technologies of tissue engineering and regenerative medicine.

ASSOCIATED CONTENT

Supporting Information

Representative frequency sweep curve of sample 5SF-50G (Figure S1). This material is available free of charge via the Internet at http://pubs.acs.org.

AUTHOR INFORMATION

Corresponding Author

*E-mail: sghosh08@textile.iitd.ac.in.

Notes

The authors declare no competing financial interest.

ACKNOWLEDGMENTS

This study was supported by a Fast Track grant from the Department of Science and Technology, Government of India, and funding from the Planning Unit of IIT Delhi.

REFERENCES

(1) Barry, R. A.; Shepherd, R. F.; Hanson, J. N.; Nuzzo, R. G.; Wiltzius, P.; Lewis, J. A. *Adv. Mater.* **2009**, *21*, 1−4.
(2) Ghosh, S.; Parker, S. T.; Wang, X.; Kaplan, D. L.; Lewis, J. A. *Adv. Funct. Mater.* **2008**, *18*, 1883−1889.
(3) Murphy, A. R.; Kaplan, D. L. *J. Mater. Chem.* **2009**, *19*, 6443−6450.
(4) Furth, M. E.; Atala, A.; Dyke, M. E. V. *Biomaterials* **2007**, *28*, 5068−5073.
(5) Hersel, U.; Dahmen, C.; Kessler, H. *Biomaterials* **2003**, *24*, 4385−4415.
(6) Chang, C. C.; Boland, E. D.; Williams, S. K.; Hoying, J. B. *J. Biomed. Mater. Res.* **2011**, *98B*, 160−170.
(7) Lai, J. Y. *J. Mater. Sci. Mater. Med.* **2010**, *21*, 1899−1911.
(8) Ofner, C. M.; Bubnis, W. A. *Pharm. Res.* **1996**, *13*, 1821−1827.
(9) Gil, E. S.; Spontak, R. J.; Hudson, S. M. *Macromol. Biosci.* **2005**, *5*, 702−709.
(10) Ghosh, S.; Laha, M.; Mandal, S.; Sengupta, S.; Kaplan, D. L. *Biomaterials* **2009**, *30*, 6530−6540.
(11) Bigi, A.; Cojazzi, G.; Panzavolta, S.; Rubini, K.; Roveri, N. *Biomaterials* **2001**, *22*, 763−768.
(12) Gil, E. S.; Frankowski, D. J.; Hudson, S. M.; Spontak, R. J. *Mater. Sci. Eng. C* **2007**, *27*, 426−431.
(13) Hu, X.; Kaplan, D.; Cebe, P. *Macromolecules* **2006**, *39*, 6161−6170.
(14) Kuijpers, A. J.; Engbers, G. H.; Krijgsveld, J.; Zaat, S. A.; Dankert, J.; Feijen, J. *J. Biomater. Sci. Polym. Ed.* **2000**, *11* (3), 225−43.
(15) Parker, S. T.; Domachuk, P.; Amsden, J.; Bressner, J.; Lewis, J. A.; Kaplan, D. L.; Omenetto, F. G. *Adv. Mater.* **2009**, *21*, 2411−2415.
(16) Shepherd, J. N. H.; Parker, S. T.; Shepherd, R. F.; Gillette, M. U.; Lewis, J. A.; Nuzzo, R. G. *Adv. Funct. Mater.* **2011**, *21*, 47−54.
(17) Russo, A.; Ahn, B. Y.; Adams, J. J.; Duoss, E. B.; Bernhard, J. T.; Lewis, J. A. *Adv. Mater.* **2011**, *23*, 3426−3430.
(18) Terry, A. E.; Knight, D. P.; Porter, D.; Vollrath, F. *Biomacromolecules* **2004**, *5*, 768−772.
(19) Boulet-Audet, M.; Vollrath, F.; Holland, C. *Phys. Chem. Chem. Phys.* **2011**, *13*, 3979−3984.
(20) Lu, Q.; Zhu, H.; Zhang, C.; Zhang, F.; Zhang, B.; Kaplan, D. L. *Biomacromolecules* **2012**, *13*, 826−832.
(21) Jetbumpenkul, P.; Amornsudthiwat, P.; Kanokpanont, S.; Damrongsakkul, S. *Int. J. Biol. Macromol.* **2012**, *50*, 7−13.
(22) Lewis, J. A. *Adv. Funct. Mater.* **2006**, *16*, 2193−2204.
(23) Lide, D. R. *CRC Handbook of Chemistry and Physics*, 88th ed; CRC Press: Boca Raton, 2012; p 6-232.
(24) Chirgadze, Y. N.; Shestopalov, B. V.; Venyaminov, S. Y. *Biopolymers* **1973**, *12*, 1337−1351.
(25) Miyazawa, T.; Blout, E. R. *J. Am. Chem. Soc.* **1961**, *83*, 712−719.
(26) Gil, E. S.; Frankowski, D. J.; Bowman, M. K.; Gozen, A. O.; Hudson, M.; Spontak, R. J. *Biomacromolecules* **2006**, *7*, 728−735.

(27) Wray, L. S.; Hu, X.; Gallego, J.; Georgakoudi, I.; Omenetto, F. G.; Schmidt, D.; Kaplan, D. L. *J. Biomed. Mater. Res. Part B: Appl. Biomater.* **2011**, *99B*, 89−101.
(28) Lu, Q.; Hu, X.; Wang, X.; Kluge, J. A.; Lu, S.; Cebe, P.; Kaplan, D. L. *Acta Biomater.* **2010**, *6*, 1380−1387.
(29) Stokes, D. G.; Liu, G.; Dharmavaram, R.; Hawkins, D.; Piera-Velazquez, S.; Jimenez, S. A. *Biochem. J.* **2001**, *360*, 461−470.
(30) Watanabe, H.; Yamada, Y.; Kimata, K. *J. Biochem.* **1998**, *124*, 687−693.
(31) Choi, C. K.; Breckenridge, M. T.; Chen, C. S. *Trends Cell Biol.* **2010**, *20*, 705−714.
(32) Woods, A.; Wang, G.; Beier, F. *J. Biol. Chem.* **2005**, *280*, 11626−11634.
(33) Woods, A.; Wang, G.; Dupuis, H.; Shao, Z.; Beier, F. *J. Biol. Chem.* **2007**, *282*, 23500−28508.